About the reliability of EBSD measurements: Data enhancement

IOP Conf. Series: Materials Science and Engineering **891** (2020) 012018 doi:10.1088/1757-899X/891/1/012018

About the reliability of EBSD measurements: Data enhancement

G Nolze[1] and A Winkelmann[2]

[1] Federal Institute for Materials Research and Testing (BAM), Unter den Eichen 87, 12205 Berlin, Germany
[2] AGH - University of Science and Technology, Academic Centre for Materials and Nanotechnology, Al. Mickiewicza 30, 30059 Krakow, Poland

E-mail: gert.nolze@bam.de

Abstract. An extensive set of information about the diffracting volume is carried by EBSD patterns: the crystal lattice, the reciprocal lattice, the crystal structure, the crystal symmetry, the mean periodic number of the diffracting phase, the source point from where it has been projected (projection centre), the crystal orientation, the sample topography (local tilt), the (preparation) quality or defect density of the crystal, and possible pattern overlaps. Some of this information is used regularly in conventional EBSD analyses software while others are still waiting for a more widespread application. Despite the wealth of information available, the accuracy and precision of the data that are presently extracted from conventional EBSD patterns are often well below the actual physical limits. Using a selection of example applications, we will demonstrate the gain in angular resolution possible using relatively low-resolution patterns of approximately 20k pixels in combination with pattern matching (PM) approaches. In this way, fine details in a microstructure can be revealed which would otherwise be hidden in the orientation noise.

1. Introduction

Electron backscatter diffraction (EBSD) is a technique for a quantitative microstructure characterisation of crystalline materials in the scanning electron microscope (SEM). Standard applications use EBSD patterns primarily to identify phases, phase distribution, texture description, grain size, grain shape and grain boundary analysis. New data-processing tools are continuously developed, and these can help to improve the reliable interpretation of often very complex microstructural problems in materials science.

Because small misorientations (MO) are important for understanding the mechanical behaviour of materials [1–3], it is important that the EBSD orientation measurements are precise. The computation of the MO can be performed by multiplying only two orientation matrices: $\mathbf{\Delta g}_{ij} = \mathbf{g}_i^{-1} \bullet \mathbf{g}_j$, from which the MO angle and axis can be determined.

A key factor for orientation and MO measurements is the angular resolution, which determines the precision of a crystal orientation derived from an EBSD pattern. Indirect techniques are common to determine the MO precision, e.g., the determination of MOs measured under comparable conditions at two positions in an undeformed grain. As these positions are presumed to have negligible MOs, the apparent MOs can be used to approximate an error of the experimental MO determination. From the accompanying MO histogram, the mean, the maxima, or the 95th percentile of the MO distribution can be interpreted as alternative measures for the orientation error.

Of widespread use is kernel average misorientation (KAM) angle which is the mean deviation of orientations determined around a selected pixel to the orientation of the pixel itself. Please note that this approach additionally reduces the real, or relative, orientation variation by the orientation averaging. Moreover, the definition of the kernel size for local averaging is different from software to software packages so that KAM angle distributions are only comparable if the same algorithm and parameters (maximum MO angle, number of classes, etc.) were used. In the present paper we use the KAM as calculated in MTEX [4] which is based on four surrounding pixels and a central pixel (top, bottom, right and left).

Approaches for an increase of the angular resolution in EBSD have been previously discussed, see e.g., [5]. From simple geometrical reasons it can be expected that the acquisition of higher-resolved, i.e., less-binned EBSD patterns, should be a straightforward way to increase the angular resolution of the orientation results. This more time consuming measurement effort for a higher pattern resolution is not always practical and can result in less precise results, cf. Fig. 1. In this context, it is unfortunate that the specific post-processing procedures in commercial "black-box" software are usually inaccessible. The graphs in Fig. 1 display the KAM angle distributions for maps derived from EBSD patterns with different image resolution of 160 × 115 and 320 × 230 pixels in addition to those obtained from different Hough-resolution. As anticipated, the higher the image resolution the higher the angular resolution, i.e., the blue curve shifts to smaller misorientation angles. However, to obtain this higher resolution with comparable signal quality, the dwell time must be quadrupled for 320 × 230 pixel patterns. Please note that the red curve in Fig. 1 is also derived from low-resolved patterns, but collected with effectively the same total exposure time because of the application of frame averaging: $t_{320\times230}$ = 4frames • $t_{160\times115}$. Taking into account that the blue and red curve were taken at different mapping positions, their similar shapes suggest an apparent correlation between pattern and angular resolution. Because of the identical measurement times but different pattern resolutions, the similarity of the KAM results indicates a software-internal, further binning of patterns to a general size and resolution. The detectable but small increase in orientation precision is very likely the result of an unintentional improvement of signal-to-noise ratio by software-internal binning and not related to the selected pattern resolution.

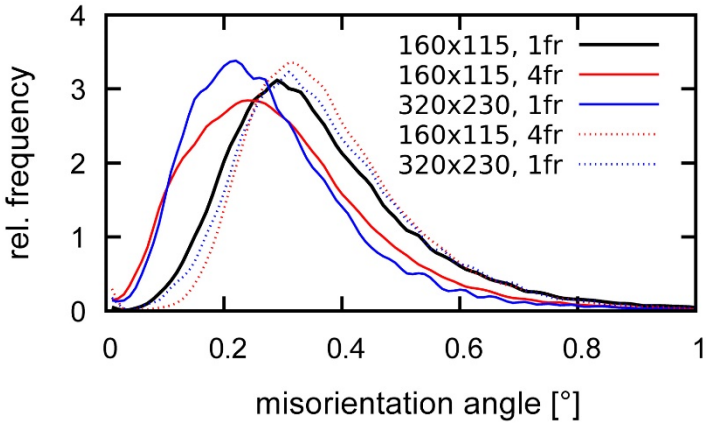

Figure 1. KAM angle distribution (polycrystalline GaP). Patterns of 320 × 240 pixel size deliver a slightly better angular resolution than 160 × 120 pixel patterns, but four frames (fr) averaged generate an equivalent distribution as the higher resolved patterns. Hough-resolution (HR) indexing using HR = 100 (dotted lines) versus the default value of HR = 60 (solid lines).

The analysis discussed above has been performed using the default Hough resolution of HR = 60 in CRYSTALIGN (Esprit 1.94, Bruker-Nano). It can be expected that an increase of the Hough space resolution HR should actually deliver a higher angular precision since it resolves the Hough space with a considerably higher resolution. As can be seen in Fig. 1, however, an increase to HR = 100 results in a histogram which is effectively identical to the one performed in a quarter of time, cf. the identically coloured, dotted lines.

While the need for higher angular resolutions in EBSD is a permanent issue, it is interesting to observe the actual improvements in orientation resolution when higher-resolved patterns are collected. In [6] patterns of 640 × 480 pixels and 128 × 96 pixels have been used for comparative measurements in deformed stainless steel. Relative to the 16-times longer acquisition time for the non-binned patterns, the achieved improvements are quite small. In [7] it is reported that the derived average geometrically necessary dislocation (GND) density seems to be unaffected by pattern resolutions higher than 160 × 128 pixels. These results are possibly related to the software-internal pattern processing discussed above. In [8, 9] the mean of the KAM distribution was two times smaller for the 640 × 480 pixel size as compared to the 128 × 96 pixel size (step size: 250 nm). This difference continues to decreases with increasing step size. For 3 µm step size, high-resolution patterns are only ≈5 % more precise than their low-resolution equivalent.

In [7] the influence of the step size (map resolution) on GND and MO fluctuation has also been investigated. In order to exclude the dependency of step size in the local deformation assessment, a parameter called the local gradient G(L) was proposed [10]. In summary, it can be stated that an increase or even an estimation of the orientation correctness without exact knowledge of the company-specific techniques used during pattern processing is not target-oriented. An independent technique is needed that re-analyses the diffraction patterns as unaffected data sources.

2. Orientation refinement by pattern matching

Pattern matching (PM) is an orientation refinement which starts with a crystal orientation taken from a conventional EBSD system, and tries to find a more precise orientation description by optimising the match between the locally acquired experimental and in real-time simulated patterns. Depending on the required resolution, this process can be much more time consuming in comparison to the Hough-based orientation determination. However, the primary goal of PM is not a further increase of measurement speed but a higher orientation precision. In this way, PM approaches can be an additional tool for applications where conventional EBSD does not have enough resolution or fails completely.

2.1. Small MOs with high precision

The first example uses a duplex steel which contains austenite precipitates in a ferrite matrix that are formed during heat-treatment. The mapped area shown in Fig. 2 is smaller than the ferrite grain so that all precipitates are orientation variants of this specific ferrite grain. For materials engineering, the most accurate description of the orientation relationship as well as the habit plane are of high interest since it is assumed that they correlate directly with the strength of the material. Therefore, a highly precise orientation measurement is desired in this case.

The KAM angle maps in Fig. 2 already indicate a clear improvement compared to the manufacturer result. The reddish coloured map in Fig. 2a changes to a much lighter coloured image in Fig. 2b. The latter also enables a clear recognition of the austenite precipitates.

The respective histograms of the KAM angle in Figs. 2c and 2d reflect quantitatively the increase in orientation precision. The according maxima, mean values and ranges which cover ≈ 95 % of all KAM angles are listed in Table 1. All values are at least four-times smaller which is interpreted as significant improvement of the orientation precision. This effect is also evident in pole figures which display the pole distribution of approximately 66,000 single austenite measurements. The scattering of the approximately displayed 400,000 dots is already small for the raw orientation data, but for the refined orientations the pole scattering is considerably reduced. Thus, the pole distribution looks sharper.

Beside the higher precision, PM has still another benefit. In about 200 out of 268,000 cases, the commercial EBSD system failed in the phase assignment, cf. the extra dots in the centre of one segment of the three-fold symmetric pole distributions in Fig. 3a. Using PM, the software realises the low correlation between the assumed phase and the locally acquired backscattered Kikuchi diffraction (BKD) pattern (EBSD patterns corrected by the background signal). A test with ferrite patterns showed they fit clearly better.

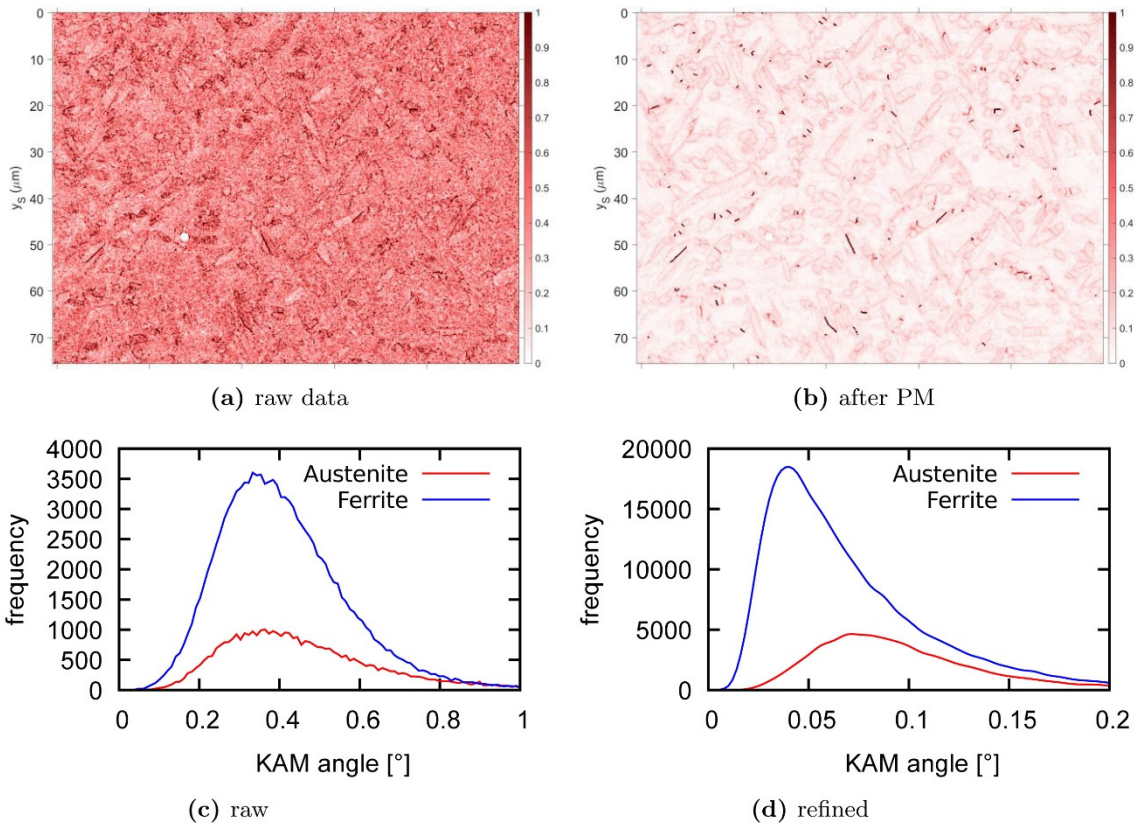

(a) raw data **(b)** after PM

(c) raw **(d)** refined

Figure 2. a) KAM angle maps derived from raw orientation data (ESPRIT 1.94, Bruker), and b) from refined orientation data after PM. The respective histogram plots are shown in c) and d). Please note the different KAM angle scales in c) and d).

Table 1. Some characteristic parameters of the KAM angle distribution from Fig. 2. The difference between raw and refined data are roughly described by a factor 4.

		maximum	mean	≈ 95 %
raw	austenite	0.36°	0.43°	0.89°
	ferrite	0.33°	0.39°	0.71°
refined	austenite	0.08°	0.09°	0.20°
	Ferrite	0.04°	0.06°	0.16°

This example demonstrates that even EBSD patterns with a comparatively low resolution of only 160 × 115 pixels possess a high orientation precision. As a matter of course, the degree of improvement depends on many factors. For ideal materials with low dislocation or defect density, like Si, the precision can reach factors of up to 10. However, as defect density increases the improvement factor in the KAM angle histogram is lowered since the histogram broadening is dominated by intrinsic misorientations and not by the orientation noise. Nevertheless, even in such cases the precision of PM is still incredible as visible on the microstructure of the next application.

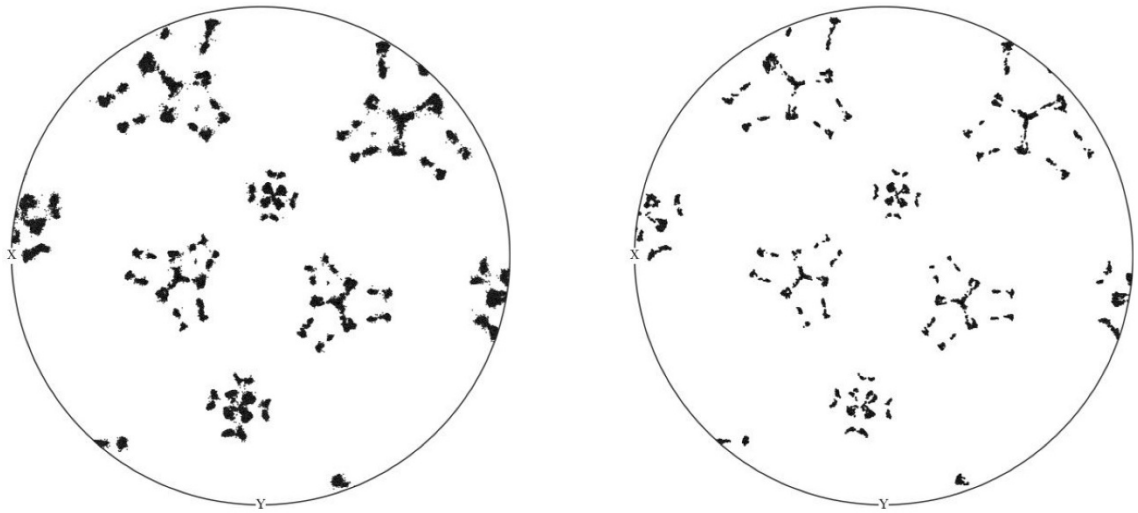

(a) 66464 raw orientations **(b)** 66273 orientations after PM

Figure 3. a) {011} pole figures derived from raw orientations, and b) from orientation data after PM. The reduction of scattering from a) to b) is satisfying. The number of considered measured points differs since during refinement PM realises that for ≈ 0.07 % of all measurements the phase was wrongly identified.

2.2. Large misorientations at high precision

The development of new materials or manufacturing processes often triggers a number of complications since previously used test and analytical procedures probably need to be adapted in order to discover new characteristic features and novel correlations between microstructure and observed properties. Additive manufacturing (AM) proposes a promising technology which generates totally different and unusually complex and variable microstructures.

Typical characteristics of AM are repetitive remelting, fast local cooling and an extremely heterogeneous and complicated structure derived from the applied (sequential) printing-like technique. Thus, features like a periodically varying grain size distribution, or comparatively strong lattice rotations are not surprising. The gradient defined by the microscopic, “lattice-like” periodic printing technique places higher demands on area selection (target preparation) as well as on test methods. Terms like “statistically relevant” will take on an entirely new dimension since “uniform” or “regular” are microstructure properties which no longer match to this technology.

Nevertheless, as technique with high spatial resolution, EBSD is a recommendable analytical method. It is only the angular resolution required for a precise evaluation of existing lattice rotations that needs improvement. On the other hand, the formed microstructure in AM materials is characterised by comparatively big lattice rotations. A suitable visualisation is the grain reference orientation deviation (GROD) angle which displays the angular deviation of the local orientation to the mean orientation of the grain, cf. Fig. 4. It represents a top view on the printed material. The periodicity in the checkerboard-like microstructure is consistent with the printing process but not identical since they are shifted against each other by one half. This means that the printing path is defined by the clearly visible boarder lines of the checkerboard and not by the centres of the visible squares. The colour bar in Fig. 4 suggests that 7° or more is a commonly observed misorientation angle. Thus it may be that high orientation precision is not required for AM materials.

In order to discuss this issue, Fig. 5 compares the KAM maps based on conventional and refined orientation data. Despite huge lattice rotations accumulated during fast solidification, both KAM maps display significant differences. The lower orientation noise in Fig. 5b enables a more authentic

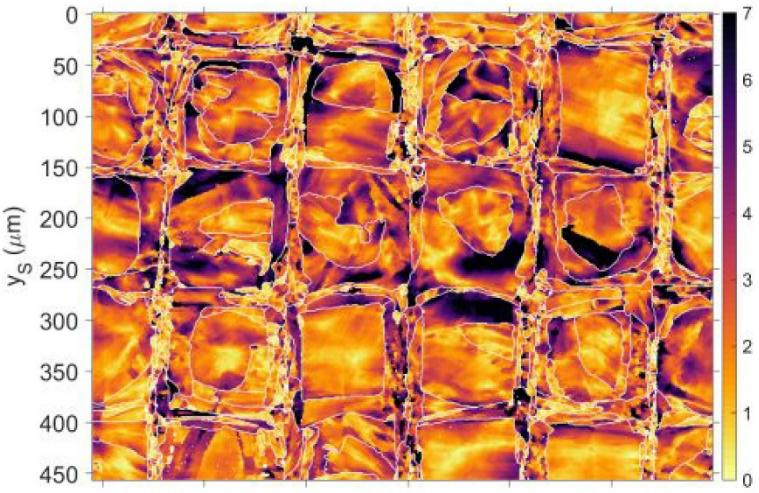

Figure 4. GROD angle map (in degrees) reflecting considerable lattice rotations within additive manufactured material. Grain boundaries are overlaid as white lines.

impression on information which are, of course, also intrinsic in Fig. 5a. It is only because of the high orientation noise that they are not observed. This difference suggests that a high orientation precision is also beneficial in case of big lattice rotations since they enable a reliable evaluation of low-angle boundaries, although the inhomogeneity of the square-shaped regions underlines the complexity of any interpretation of such processes. They have neither the translation symmetry (homogeneous) within the observed surface plane nor in depth.

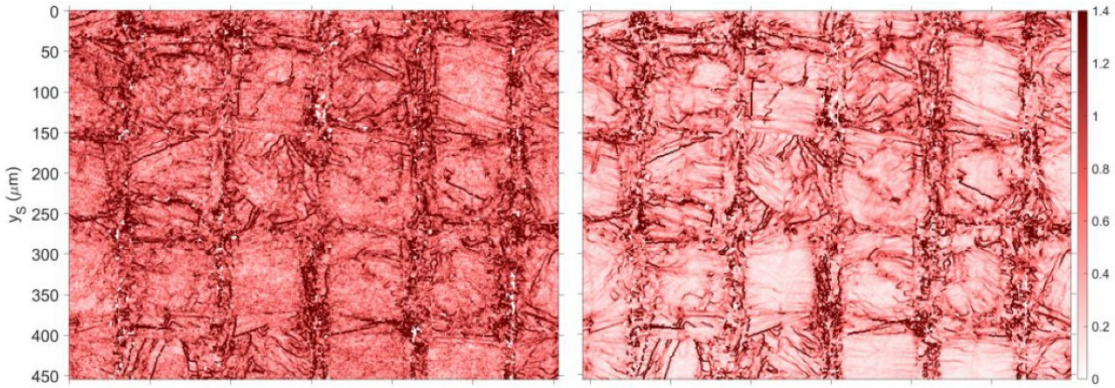

Figure 5. Comparison of KAM angle maps. The raw orientation a) enables the recognition of low and high defective regions; however, the higher precision in b) extracts much more details which cannot be discovered in a).

As mentioned above, the high precision of PM is not that evident anymore in KAM angle distributions when other effects like a high intrinsic defect density dominate the curve shape, cf. Table 2. Although the maximum and mean for the refined data differ by a factor of two, the 95 % range does not appreciably change due to the big lattice rotations within grains.

A reliable detection of small misorientations is preferably interesting for a more advanced interpretation. A typical application is the density of GNDs [11]. For the derivation of the curvature tensor a clear qualitative leap is apparent by PM, cf. Fig. 6. This gives at least some prospects regarding a more reasonable characterisation of high-gradient materials so that the data significantly contributes to a better understanding and a successful correlation between microstructure and material properties.

Table 2. Some characteristic parameters of the KAM angle distribution derived from Fig. 5

	maximum	mean	≈ 95 %
raw	0.58°	0.70°	1.64°
refined	0.28°	0.40°	1.49°

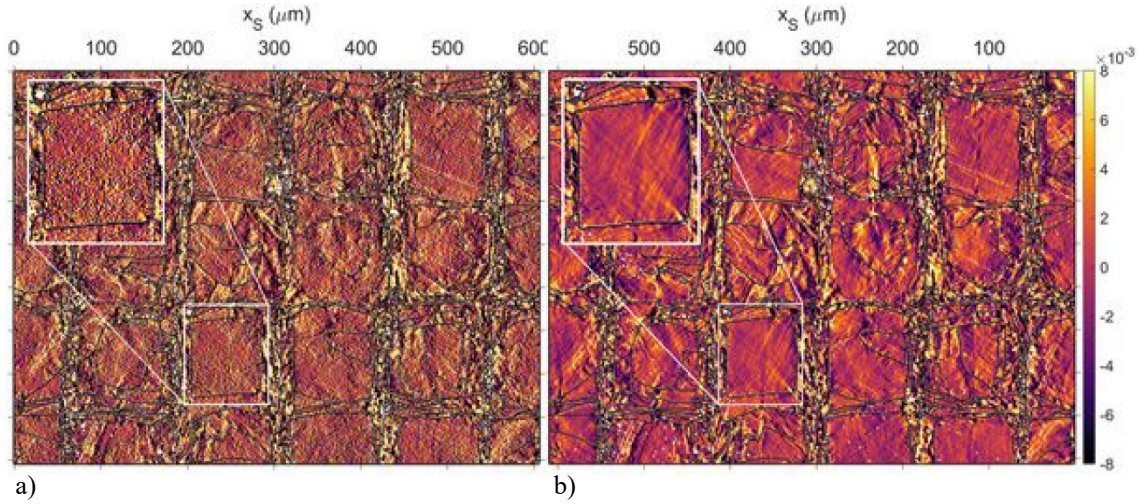

Figure 6. One of the six measurable components of the EBSD curvature tensor $\boldsymbol{\kappa}$ – $\boldsymbol{\kappa}_{31}$ – which is used for the computation of the GND density. Both maps are derived from the identical patterns, only a) shows the result from raw orientations, whereas in b) the refined orientation data are used.

2.3. Pseudosymmetric crystal lattices

Phase transformation is a common phenomenon in material science. During this process, the atomic configuration at lower temperature tends to loose the previously higher symmetry by small shifts of atoms. Although such movements do not practically vary the intensity of bands, they are associated with a slight deformation of the crystal lattice and may require a redefinition of the basis vectors which results in clearly different lattice parameters.

Quite frequently observed is the transition from a hexagonal close-packed arrangement of statistically distributed or already ordered elements to a further ordered configuration with longer translation periodicity of orthorhombic symmetry. As one representative Ni_3Sn_2 shall be discussed. The lattice relationships are summarised in Table 3. The last row shows that during phase transformation the lattice effectively contracts in maximum only 1.7 % which is below the typical detection limit of EBSD, at least for the low-resolution patterns. To be on the safe side, for this investigation patterns of 400 × 300 pixels have been used. Later measurements demonstrated that this pseudosymmetric problem can be solved by EBSD patterns in lower resolution (160 × 115 pixels).

A single grain of Ni_3Sn_2 decomposes into numerous domains during cooling which have crystallographically three totally different orientations of pseudosymmetric character. This means that despite non-equivalent orientations the respective diffraction signals look nearly identical. Therefore, the indexing fails and randomly one of the three pseudosymmetric orientations are selected by the software. Notwithstanding that fact, the domains can be easily imaged by channelling-in contrast in SEM [12]. The question arises regarding the reliability of PM to discriminate between these three orientation variants.

Table 3. Lattice correlations of high (HT) and room temperature (RT) phase of Ni_3Sn_2. V_{uc} … unit cell volume.

	Ni_3Sn_2 (HT)	Ni_3Sn_2 (RT)
symmetry	$P\,6_3/mmc$	$P\,nma$
lattice parameters	$a_h = 4.146\,\text{Å}$ $c_h = 5.253\,\text{Å}$	$a_o = 7.124\,\text{Å}$ $b_o = 5.195\,\text{Å}$ $c_o = 8.152\,\text{Å}$
V_{uc}	$75.5\,\text{Å}^3$	$304.9\,\text{Å}^3 \approx 4 \cdot V_{uc_h}$
relationships		$a_o \approx \sqrt{3} \cdot a_h \quad (-0.8\%)$ $b_o \approx c_h \quad (-1.1\%)$ $c_o \approx 2 \cdot a_h \quad (-1.7\%)$

As Fig. 7 (a) demonstrates by the three different colours, a separation of the pseudosymmetric orientations is possible and also reliable. However, compared to the standard PM the applied procedure works a bit different. As usual, the refinement starts with the orientation delivered from the EBSD system. This can be either an orientation based on the orthorhombic low-temperature unit cell, or anorientation based on the high-temperature hexagonal lattice. Both have drawbacks since the $\vec{c}$-axis of the hexagonal phase is not parallel the $\vec{c}$-axis of the low-temperature phase but to the $\vec{b}$-axis, cf. Table 3. Therefore, several transformations are necessary to derive respective projections from the orthorhombic template pattern using orientations referring to a hexagonal cell. An easier method uses a refinement based on pseudosymmetric data of the orthorhombic phase. However, now $\vec{b}$ as monoclinic axis does not match the Euler-angle convention rotating around Z and X, respectively $\vec{e}_3$ and $\vec{e}_1$. Notwithstanding these complications, the subsequent refinement compares the match for all three pseudosymmetric solutions. The best is taken as most likely orientation description for this pattern. The briefly sketched procedure not only delivers a qualitatively convincing distribution of the three variants, but also satisfies in a quantitative manner. This is first demonstrated in Fig. 7b by the KAM angle distribution. For the shown map 95 % (blue line) of all derived KAM angles are smaller than 0.14° with a median (green line) of 0.04° which is certainly the main impact of higher-resolved patterns analysed.

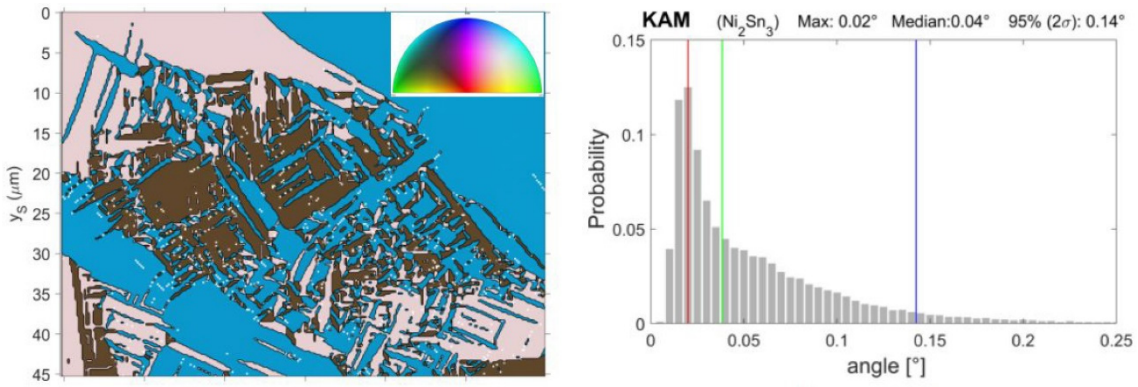

a) IPF-X map b) after PM

Figure 7. Orientation description of Ni_3Sn_2-domains covering three pseudosymmetric orientations within a former single grain. The orientation description is based on the enantiomorphic symmetry group 222 [13].

Despite these small KAM angles, MOs not only result from orientation noise but also from real existing lattice rotations. For the imaging of the MO we will now use the GROD angle, as in Fig. 4 in addition to the MO axis which transfers the local orientation in the mean orientation of the grain by a rotation around the GROD angle. The maps displaying the GROD angles and axes are pictured in Fig. 8. The colour bar of the GROD angle encodes an angle variation between 0 … 1°. The colour distribution in Fig. 8a shows that large areas are characterized by GROD angles < 0.2°. Despite these small angles, the noise is reduced in the map which indicates a high orientation precision in agreement with the KAM angle histogram in Fig. 7. The map also proves that within comparatively big grains higher GROD angles may occur. They mainly appear in correlation to other variants which is not surprising since transformations with lattice distortions are assumed to cause stress which may result in small lattice rotations.

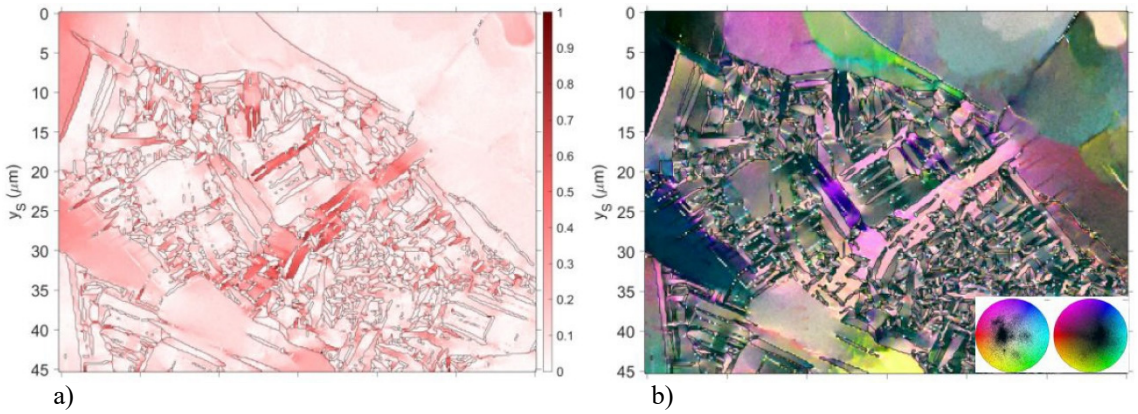

Figure 8. Grain reference orientation deviation (GROD) displayed as a) rotation angle, and b) as rotation axis. The inset image in b) displays the MO axes distribution as stereographic projection of the two hemispheres.

The MO angles help to understand and imagine the reaction of a microstructure on processes like transformations. In many cases the MO axis is of high interest, especially when the directional distribution is inhomogeneous. If no correlation to the crystal symmetry is assumed, a rotation direction colouring of the entire projection sphere needs to be considered, cf. the inset image in Fig. 8b. Many directions form a point cloud within the upper hemisphere (left) displaying as well the colour key. In contrast to the pure MO angle presentation, the colouring of the MO axis results in clearly higher colour contrasts. Please note that small MO angles commonly result in a considerable uncertainty of the MO axes. In this respect, the comparatively low colour fluctuation in Fig. 8b is surprising. In any case, it is a further indication for the high orientation precision achievable with PM.

Both the MO axis and angle, can be processed together when the used colour key is compressed so that for each specific grain the orientation variation is used to define the colour key size. Then identical MO angles are differently coloured when their MO axes varies as shown in Fig. 9.

Please note that the centre of gravity of the (compressed) colour key is defined by the mean orientation of each particular grain. The deviation of GROD angle as well as GROD axis is used to assign the colour. The disadvantage of this presentation tool is that an interpretation is only qualitatively possible since the definition of each colour depends on the compression applied.

Another domain-forming phase is perovskite. It is in fact a materials class which is characterised by numerous phase transitions describing different crystallographic subgroup relationships. Thus, in addition to the ideal cubic structure type, all other crystal systems down to triclinic phase descriptions can be found in databases. However, most of the listed phase descriptions are so similar that even X-ray

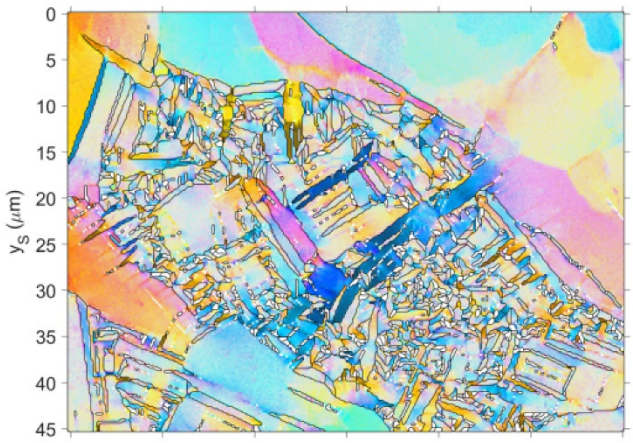

Figure 9. MO angle and axis from Fig. 8 encoded by a heavily compressed IPF-colour key. The orientation spread (polar angle) needs to be manually adapted.

powder diffraction as standard tool for phase discrimination cannot distinguish between them. Since the ability to distinguish between phases is reduced for EBSD, any attempt to try this for pseudo-cubic perovskite is doomed to failure. A safe option is to use channelling-in contrast in SEM, or FSE images to recognise non-cubic perovskites by the characteristic herringbone structure, cf. Fig. 10. This is indisputable evidence that a perovskite is not of cubic symmetry and the lattice is slightly distorted. Figure 10 displays a bimodal microstructure of coarse $BaTiO_3$ crystals embedded in a fine-grained matrix. The most often used approach in case of domains is a tetragonal distortion described by a c/a ratio very close to 1.

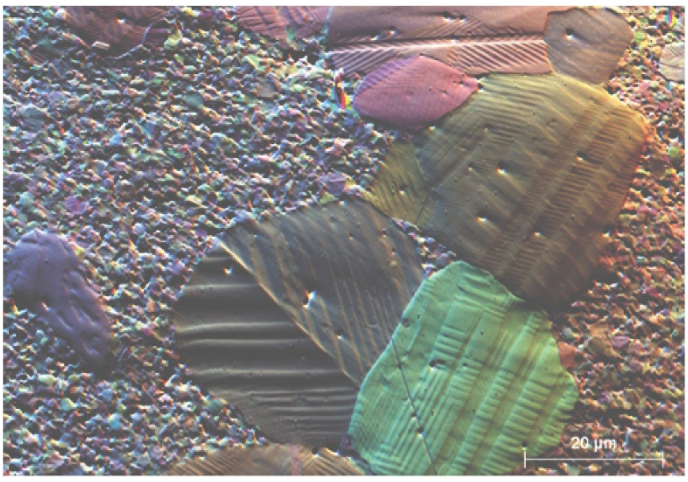

Figure 10. Forescattered electron image of a $BaTiO_3$ ceramic reflecting the characteristic herringbone structure. Please note the different colours of the grains whereas the domains do not considerably vary in colour but mainly in topography.

EBSD investigations prove that all BKD patterns can be easily indexed using a cubic crystal description. A single grain is then reflected as uniform crystal, possibly with a thin twin lamella, cf. for two of the four biggest grains in Fig. 10. In contrast, the attempt to index the patterns by a tetragonal phase description results in a more or less random selection of pseudosymmetric orientation solutions, as reported above for Ni_3Sn_2. Sometimes the indexing delivers a preferable selection of an orientation solution for a few domains, but after rotating the sample by a few degrees only this preferred orientation selection disappears so that it is assumed to be an artefact of the applied band detection.

For PM we used a similar approach as briefly sketched for Ni_3Sn_2, only that now all axes are consistent ($\vec{c}_{cub} \| \vec{c}_{tet} \| \vec{e}_3$), and only three pseudosymmetric solutions exist. The IPF-map in Fig. 11a proves that obvious misinterpretations do not occur. On the first glance, domains are uniformly indexed in a way which appears reasonable.

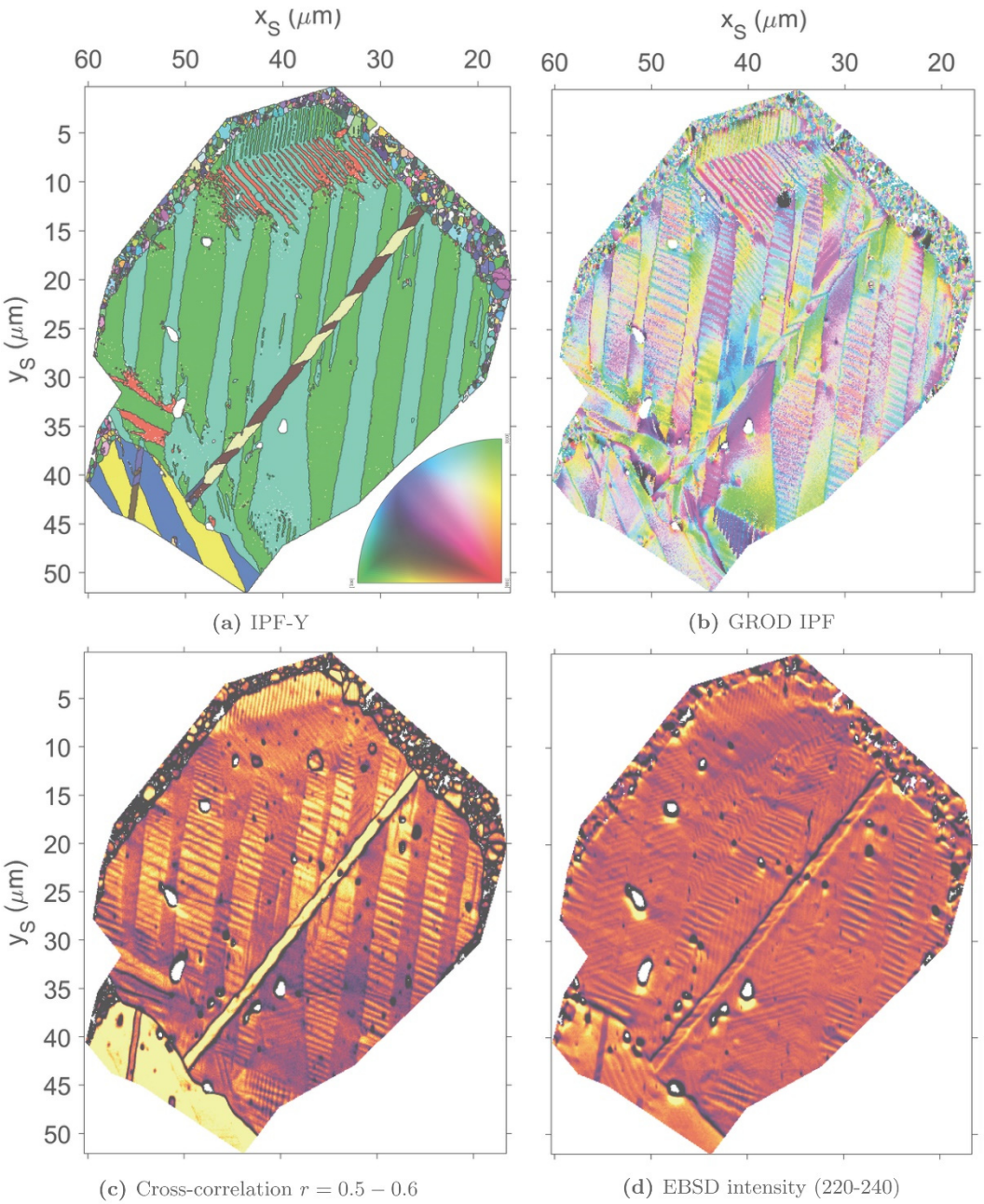

Figure 11. Orientations in a tetragonally assumed $BaTiO_3$ derived by PM and displayed as IPF-Y map. For the sake of clarity grain boundaries are displayed as black lines (a). The intragranular misorientations are imaged in b) by a compressed IPF-colour key which displays systematic orientation variations within uniformly assumed domains in (a). In order to compare the information content the cross-correlation coefficient (c) and the overall intensity derived from the EBSD patterns (d) are shown as well.

However, a comparison with FSE images raises at least tentative doubts that the displayed unambiguousness in grain recognition is totally correct. The reason for qualms is the discrepancy between the numerous domains visible in FSE images and the apparent uniformity in the IPF map. In other words, the big domains look too uniform.

According to the doubts, further investigations of possible MOs discover a systematic orientation modulation which suggests a correlation to the domains visible in FSE images like in Fig. 10. Despite the comparatively noisy signal, the modulation in form of parallel and practically equidistant stripes are well visible, see Fig. 11b. It is, however, conspicuous that there is no overall correlation. Fortunately, the differing regions accidentally correlate with the four biggest pores visible in the maps. Whereas in Figs. 11b and 11c the slope of the faintly visible, thin stripe are uniform from left top to right bottom, in Fig. 11d they are reverse. Due to this, the question is posed more and more often, whether for the different maps in Fig. 11 the identical information from EBSD patterns is used. Figs. 11a and 11b are based on the derived orientation solution only.

Figure 11c represents the map which indicates the degree of match used for Figs. 11a and 11b. Brighter colours indicate a better correlation whereas darker colours suggest that the applied PM resulted in a lower cross-correlation value *r*. Reasons for the signal differences in Fig. 11c may be related to the orientation description or to an unfortunately selected phase description having an imperfect *c*/*a* ratio. The map in Fig. 11d, however, is mainly triggered from the background intensity. Since the chemical composition is uniform, only channelling-in and topography are the main influencing factors. The signal in Fig. 11d is formed in higher depths so that we assume that the different slope has its reason in different information depths of BKD and background signal.

Another factor which should be considered is the influence of the angular resolution due to the sample tilt in combination with the domain alignment. For different alignments in depth the interaction volume reacts in a smearing which fits to the nearly homogeneously but darker coloured domains in Fig. 11c. In between domains show higher *r*-values, which suggests that they are favourably aligned and the electron probe does not average differently aligned domains as in the neighbourhood. The darker stripes are explainable by thin subdomains which produce an overlaid signal of two different but pseudosymmetric orientations. The impact of the spatial resolution at tilted sample surfaces can be also seen at the upper part of the crystal, cf. Fig. 11c. There, a herringbone structure of very fine domains can be observed with conventional EBSD. All different domains can be distinguished but the signal for the nearly vertically aligned domains at the top of the image is of much higher quality since in Fig. 11c they show higher *r*-values than the domains directly below in the image.

3. Summary and conclusions

In the selected examples that were presented, the potential of low-resolution (10k - 20k pixels) EBSD patterns was demonstrated to improve of orientation precision. In order to circumvent the unknown image processing of high-resolved patterns in the manufacturer software, pattern matching (PM) of stored pattern with dynamical simulations was used. The orientation data derived from the low-resolution EBSD patterns are already of higher precision than comparable investigations based on higher resolved patterns with Hough-based orientation determination. It has been shown that a higher precision can be useful for the investigation of materials with different levels of deformation. PM offers the highest precision, required in the case of discriminating pseudosymmetric orientation solutions.

While combination of higher-resolved patterns and PM can improve the orientation precision, other influences then start to become important such as: varying lattice parameter ratios, the correct projection centre position, the possible pattern distortions caused by local magnetic or electric fields, and the effective electron energy.

Acknowledgement

We are very thankful for being able to investigate the duplex steel sample provided by W. Swiatnicki (TU Warsaw). We thank K. Sommer (BAM Berlin) for the austenitic sample produced by additive

manufacturing, and A. Leineweber (TU Bergakademie Freiberg) for providing the Ni_3Sn_2 sample. In particular, we also express our gratitude to R. Saliwan Neumann and M. Buchheim for countless preparations and EBSD experiments in BAM, R. Hielscher for developing and continuous maintenance of MTEX, and J.A. Schneider (University of Alabama in Huntsville) for correcting the manuscript.

References

[1] Wilkinson A J 2001 A new method for determining small misorientations from electron backscatter diffraction patterns. *Scripta Materialia* **44** 2379-2385
[2] Bate P S, Knutsen R D, Brough I and Humphreys F J 2005 The characterization of low-angle boundaries by EBSD. *J. Microscopy* **220** 36-46
[3] Brewer L N, Othon M A, Young L M and Angeliu T M 2006 Misorientation mapping for visualization of plastic deformation via electron back-scattered diffraction. *Microsc. Microanal.* **12** 85-91
[4] Bachmann F, Hielscher R and Schaeben H 2010 Texture analysis with MTEX – Free and open source software toolbox. *Solid State Phenom.* **160** 63-68
[5] Brough I, Bate P S and Humphreys F J 2006 Optimising the angular resolution of EBSD. *Mater. Sci. Technol.* **22** 1279-1286
[6] Kamaya M 2009 Characterization of microstructural damage due to low-cycle fatigue by EBSD observation. *Mater. Charact.* **60** 1454-1462
[7] Jiang J, Britton T B and Wilkinson A J 2013 Measurement of geometrically necessary dislocation density with high resolution electron backscatter diffraction: Effects of detector binning and step size. *Ultramicroscopy* **125** 1-9
[8] Kamaya M 2009 Measurement of local plastic strain distribution of stainless steel by electron backscatter diffraction. *Mater. Charact.* **60** 125-132
[9] Kamaya M 2010 A smoothing filter for misorientation mapping obtained by EBSD. *Mater. Trans.* **51** 1516-1520
[10] Kamaya M 2011 Assessment of local deformation using EBSD: Quantification of accuracy of measurement and definition of local gradient. *Ultramicroscopy* **111** 1189-1199
[11] Pantleon W 2008 Resolving the geometrically necessary dislocation content by conventional electron backscattering diffraction. *Scripta Materialia* **58** 994-997
[12] Nolze G, Hielscher R and Winkelmann A 2017 Electron backscatter diffraction beyond the mainstream. *Cryst. Res. Technol.* **52** 1600252
[13] Nolze G and Hielscher R 2016 Orientations – perfectly colored. *J. Appl. Cryst.* **49** 1786-1802